Smith, A., Hallis, L. J., Nagashima, K. and Huss, G. R. (2020) Volatile abundances and hydrogen isotope ratios of apatite in martian basaltic breccia NWA 11522 – A paired stone of NWA 7034. *Meteoritics and Planetary Science*, 55(12), pp. 2587-2598. (doi: 10.1111/maps.13605)

The material cannot be used for any other purpose without further permission of the publisher and is for private use only.

There may be differences between this version and the published version. You are advised to consult the publisher's version if you wish to cite from it.

This is the peer reviewed version of the following article:

Smith, A., Hallis, L. J., Nagashima, K. and Huss, G. R. (2020) Volatile abundances and hydrogen isotope ratios of apatite in martian basaltic breccia NWA 11522 – A paired stone of NWA 7034. *Meteoritics and Planetary Science*, 55(12), pp. 2587-2598, which has been published in final form at: 10.1111/maps.13605

This article may be used for non-commercial purposes in accordance with Wiley Terms and Conditions for Self-Archiving.

https://eprints.gla.ac.uk/226593/

Deposited on: 4 December 2020

Enlighten – Research publications by members of the University of Glasgow
http://eprints.gla.ac.uk

Volatile abundances and hydrogen isotope ratios of apatite in martian basaltic breccia NWA 11522 – A paired stone of NWA 7034

A. Smith[1*], L. J. Hallis[1], K. Nagashima[2], G. R. Huss[2]

[1]University of Glasgow, School of Geographical and Earth Sciences, UK.
[*]Current address: The University of Manchester, School of Earth and Environmental Sciences, UK.
[2]Hawai'i Institute of Geophysics and Planetology, Pacific Ocean Science and Technology (POST) Building, University of Hawai'i, 1680 East-West Road, Honolulu, HI 96822, United States.

Abstract

This study aimed to determine the volatile content (Cl, F, OH) and hydrogen isotope (D/H) ratios of apatite grains within the martian meteorite NWA 11522, a paired stone of the ungrouped polymict breccia NWA 7034. Apatite F: Cl: OH ratios were measured via SEM-EDS analyses, and found to be strikingly similar in all grains, and dominated by Cl. Apatite D/H ratios were measured in-situ via the Cameca ims 1280 SIMS at the University of Hawaii. Results varied between δD values of 782 ‰ and 52 ‰, and water contents of between 0.127 and 0.510 wt %. The data form a mixing line between two endmembers. The first, a high D/H ratio and low water content endmember, represents a fluid present during the thermal event that lithified the breccia at 1.5 Ga, resetting apatite volatile content, D/H ratio and U-Pb ages at this time. The D/H ratio of this fluid suggests it was derived from the crust/cryosphere (e.g., melted groundwater ice). The second endmember, a low D/H ratio and high water content endmember, represents a second martian fluid that interacted with the breccia after lithification. The low D/H ratio of this later fluid indicates it was derived from the deeper martian interior, and may be evidence of an impact-related hydrothermal system on Mars during the Amazonian period. The presence of these fluids within NWA 11522 suggests that sub-surface impact crater environments were still host to liquid water during the past 1.5 Ga on Mars, and still could be to this day.

Introduction

NWA 11522 – A paired stone of Black Beauty

Until recently, Alan Hills (ALH) 84001 was the only martian meteorite that did not fit within one of the shergottite, nakhlite, chassignite (SNC) groups. However, the discovery of Northwest Africa (NWA) 7034 (Black Beauty), along with its paired stones (Santos et al., 2015) has expanded the diversity of the martian meteorite inventory on Earth (Wright et al., 2011; Agee et al., 2013; Cartwright et al., 2014; Simon et al., 2014; Shearer et al., 2015). This study focuses on NWA 11522, a paired stone of NWA 7034 (Cohen et al., 2018).

NWA 7034 was found in Morocco in 2011, and (to date) eleven additional stones have been paired with it – including NWA 11522. NWA 7034 was nicknamed 'Black Beauty' on account of its black, glassy, fusion crust (a sign of minimal terrestrial weathering). These meteorites are polymict basaltic breccias, containing a mixture of igneous, proto-breccia, and impact-processed lithic clasts, as well as single mineral clasts, within a fine-grained matrix (Agee et., 2013; Muttik et al., 2014; Goderis et al., 2016). Santos et al. (2015) reported that either lithic igneous clasts in NWA 7034 are not related (i.e., originate from separate igneous sources), or there was compositional variation within a shared parent source during formation. A range of ages have been reported for the breccia, representative of various crystallisation and resetting events (Agee et al., 2013; Lin et al., 2016; McCubbin et al., 2016a; Hu et al., 2019). U-Pb dating of a number of metamict zircon grains, and all measured apatite grains, give an age of 1.5 Ga (McCubbin et al., 2016a; Hu et al., 2019). Rb-Sr whole rock data gives an older age of 2.089 ± 0.081 Ga (Agee et al., 2013), and within some zircon grains U-Pb ages of 4.42-4.46 Ga are preserved (Lin et al., 2016; McCubbin et al., 2016a). The young apatite and metamict zircon ages can be explained via a single pervasive thermal event with temperatures of 500–800°C, evident from NWA 7034 matrix recrystallization to a fine-grained groundmass with 120° triple junction texture (McCubbin et al., 2016a). The nature of this thermal event may be volcanic pyroclastic or impact related, the presence of stishovite within the matrix of NWA 11522 indicating the latter (Daly et al., 2018). Either way, this event seems to have been that which lithified the breccia (Agee et al. 2013; McCubbin et al., 2016a).

NWA 7034 and pairs are water-rich compared to other martian meteorites, with ~6000 ppm H_2O released during bulk-rock stepped heating (Agee et al., 2013; Filiberto et al., 2019; Barnes et al., 2020). The high water content can be explained by the presence of hydrous Fe-oxide phases (e.g., goethite) and saponite phyllosilicate, as well as apatite grains (Muttik et al.,

2014; Gattacceca et al., 2014; McCubbin et al., 2016a). A number of apatite grains within NWA 7034 and paired meteorite NWA 7533 have been found to contain monazite inclusions, indicative of hydrothermal/metasomatic martian fluids interacting with chlorapatite at temperatures >100 °C (Liu et al., 2016). In contrast, the assemblage of hydrous Fe-oxides and phyllosilicates in NWA 7034, in addition to reported magnetite and maghemite, form an alteration assemblage indicative of low temperature hydrothermal alteration within these meteorites (Muttik et al., 2014; Gattacceca et al., 2014; Wittman et al., 2015). The fresh condition of NWA 7034 fusion crust, along with the oxygen isotope composition of the water within the alteration phases, suggests these low-temperature alteration phases were produced on Mars (Agee et al., 2013; Muttik et al., 2014; Wittman et al., 2015). Hence, NWA 7034 and its paired meteorites appear to have interacted with both high temperature and low temperature martian fluids.

Martian apatite as a volatile sink

Apatite [$Ca_5(PO_4)_3(F,Cl,OH)$] is the main volatile bearing igneous mineral in most martian meteorites (Greenwood et al., 2003; McCubbin and Jones, 2015; Howarth et al., 2015). Abundances of F, Cl and OH in apatite can thus be used to determine the pre-eruptive abundance of these volatiles in both their parental melts and their source regions (e.g., Mathez and Webster 2005; Patiño Douce and Roden, 2006; Patiño Douce et al., 2011; Gross et al., 2013; Filiberto and Treiman, 2009; Filiberto et al., 2016; 2019; Barnes et al., 2020), providing an insight into the volatile composition of the martian interior. However, the effects of processes such as degassing, magma mixing and/or assimilation, fractional crystallisation, and secondary alteration can change the pre-eruptive volatile content of apatite (e.g., Gross et al 2013; McCubbin et al, 2011; 2016b; Liu et al., 2016; Filiberto et al., 2019). These processes must be taken into account when attempting to calculate martian source region volatile contents.

Cl is interpreted to be the dominant volatile element in martian meteorites – martian magmas are ~2.5 × enriched in Cl compared to terrestrial magmas (Filiberto and Treiman, 2009; Filiberto et al., 2019). Orbiter and lander analysis of the martian surface also indicate Cl enrichment, with elevated levels at volcanic provinces suggesting this surface enrichment is due to volcanic degassing (e.g., Keller et al. 2006; Taylor et al. 2010). The nakhlite and chassignite meteorites in particular contain Cl-rich apatite (as well as Cl-rich amphibole in the nakhlites), reported to be the product of sub-surface interactions with a Cl-rich fluid

(McCubbin et al., 2013). The shergottites contain apatite with much more varied F: Cl: OH ratios (Filiberto et al., 2019, and references therein), reflecting the effects of degassing, magma mixing/assimilation, and fractional crystallisation, as well as differing source region volatile compositions for different shergottite groups (e.g., Barnes et al., 2020). As NWA 7034 and its paired meteorites are polymict breccias, a wide variety of F: Cl: OH ratios might be expected within separate apatite grains. However, previous studies have shown that these apatite grains are mostly Cl dominated, and link this volatile homogeneity to the thermal event at 1.5 Ga (McCubbin et al., 2016b; Hu et al., 2019).

Hydrogen isotope ratios on Mars

Martian deuterium/hydrogen (D/H) ratio measurements are standardised relative to Vienna Standard Mean Ocean Water (VSMOW), using the following equation:

$$\delta D\ (‰) = [((D/H)_{sample}/\ (D/H)_{VSMOW})] - 1]\ x\ 1000 \qquad \text{[eqn. 1]}$$

Thus, VSMOW δD = 0 ‰.

Mars has at least three separate water reservoirs, based on hydrogen isotope distinctions. The atmospheric reservoir has an extremely high δD value (2000-8000 ‰), depending on latitude (Villanueva et al., 2015) - a result of the preferential loss of the lighter hydrogen isotope to space via Jeans escape (Owen et al., 1988). Usui et al. (2015) and Usui (2019) reported the presence of an intermediate reservoir, (δD = 1000-2000‰) in the martian cryosphere/crust. This is supported by MSL curiosity measurements of Hesperian aged clay minerals at Gale crater (δD = 2000 ‰ ± 200 ‰, Mahaffy et al., 2015). The martian mantle has at least one water reservoir, with a low δD value <275‰ represented in depleted basaltic meteorites (Hallis et al., 2012; Usui et al., 2012). However, Barnes et al. (2020) recently argued that at least one additional mantle reservoir exists, represented by the high δD values within enriched shergottite apatite grains (D/H ratio = 8.03 ± 0.52 $\times 10^{-4}$, or δD = 4157 ± 666 ‰).

This study focuses on determining the volatile content and hydrogen isotope (D/H) ratio of apatite grains within NWA 11522, as a comparison to recent similar studies of NWA 7034.

Methods

Apatite volatile abundances via stoichiometric SEM-EDS analysis

Scanning electron microscope (SEM) backscattered electron images, along with energy-dispersive X-ray spectroscopy (EDS), were used to determine the texture and mineralogy of two samples of NWA 11522 (one mounted in Indium (In), the other in epoxy (Ep)). The indium mounted sample was prepared via dry polishing down to 3 microns, and then fine polishing down to 0.25 µm using diamond paste and methanol. The epoxy mounted sample was polished down to 0.25 µm using diamond paste and water. Analyses were conducted at the University of Glasgow (UoG), using the Carl Zeiss Sigma Variable Pressure Analytical SEM. Whole-sample false colour EDS montaged images (Fig. 1) were used to calculate the modal mineralogy of each sample, using the versatile wand tool within ImageJ to calculate pixel numbers for each mineral. As the pixel size for each of these images is 1 µm there is an associated uncertainty with these calculations. First, matrix minerals smaller than 1µm cannot be distinguished. Second, there is a region of uncertainty at grain boundaries that is proportionally larger for smaller grains. In addition, chemical zoning/reaction rims within individual mineral grains can produce varying results depending on which area is initially selected using the versatile wand tool. For this reason, pixel number calculations were performed five times for both samples, and a 2σ uncertainty calculated for all minerals (Table 1).

The UoG Carl Zeiss Sigma Variable Pressure Analytical SEM is capable of quantitative mineral chemistry EDS analyses, with the aid of standard materials. Operating conditions included: 15kV voltage, a beam current of 2 nA and a spot size of ~10µm. The optimal conditions recommended by Goldoff et al. (2012) for EMPA analyses of apatite are a low beam current (4 nA was the lowest tested), a 10 µm spot size and a 10 kV voltage. However, a 15 kV accelerating voltage was chosen for our analyses in order to enable detection of REEs and other trace components in apatite. This is generally standard practice for martian apatite analyses (e.g., see McCubbin et al., 2016b and references therein). Standards included apatite (for P and Ca), fluorite (for F) and tugtupite (for Cl) for chemical quantification of NWA 11522 apatite grains, with detection limits consistently <0.5 wt % for Cl and F (less for major elements). SEM-EDS analysis cannot directly measure OH, but by measuring F and Cl, the missing component (assumed to be 100 % OH) can be inferred via stoichiometry (McCubbin et al., 2011). The quality of apatite analyses was assessed based on stoichiometric constraints and analytical totals. Only analytical totals between 97–102 wt% were permitted. Analyses with lower or higher totals were discarded, consistent with the dataset of McCubbin et al. (2016b). In addition, if the stoichiometric totals for the P and Ca

sites deviated more than ± 2 % the analysis was discarded (± 0.06 structural formula units (sfu) for P and ± 0.10 sfu for Ca on a 13 anion basis). Apatite grains that were found to be stoichiometric, with an area >25 µm free of cracks or other mineral inclusions were selected for subsequent SIMS D/H analyses.

Hydrogen isotope analytical protocol

The D/H ratios of apatite grains within the two samples of NWA 11522 were analysed *in-situ* using the Cameca ims 1280 ion microprobe (SIMS) at the University of Hawai'i (UH). Prior to analysis, the two samples of NWA 11522 were placed at 60ºC in a vacuum oven for 48 hours to limit atmospheric contamination. Epoxy mounted samples are not ideal for analyses of D/H via SIMS, as the epoxy can degas inside the sample chamber, causing elevated background hydrogen levels during analysis. Unfortunately, this sample was epoxy mounted prior to the beginning of this study. However, as it was found to contain numerous large apatite grains (up to 100 µm) we decided to analyse this sample alongside the anhydrously prepared indium mounted sample. The background counts per second (cps), and the overall vacuum level, within the sample chamber were carefully monitored during each analysis, and were found to be similar for both samples. In addition, no systematic difference in water content or D/H ratio is recorded between the apatite datasets from the two samples, indicating that, in this case, the epoxy did not have a measurable affect on D/H analyses.

During analyses a focused Cs+ primary ion beam with a current of 4nA produced ions of H, D and ^{18}O. The primary ion beam was rastered over an area of 25 × 25µm for 200s, to remove any surface contamination, as well as the 15nm carbon coating. The raster area was then reduced to an analysis area of 15 × 15µm. The final spot size that data was collected from was 8 ×8µm, due to the presence of an egate excluding ions from the outer regions of the 15µm analysis raster (Hallis et al., 2015). Collection of data occurred over a period of 40 cycles. H, D, and ^{18}O were measured for 4s, 40s, and 2s, respectively. Cycles 1-9 and 36-40 were used for background collection, where the beam was blanked. Data was collected during cycles 10-35. For further details see Hallis et al. (2012). The secondary ion mass spectrometer was operated at 10 keV with a 50 eV energy window. Isotopes were detected using an electron multiplier. The mass resolving power was 2000, sufficient to separate any interfering molecules. A normal-incidence electron flood gun was used for charge compensation.

Hydrogen isotope data processing

Ion probe data is recorded in counts per second (cps). This raw data is corrected for both deadtime and background. Background was measured during the first 10 and last 5 cycles of each measurement as previously stated, which was subtracted from the isotopic data, measured during cycles 10 and 35. To correct for instrumental mass fractionation two apatite standards were used: Crystal Lode ap005 and Russia ap018 (see McCubbin et al., 2012, and supplementary online materials). Standards were measured at the beginning and end of each analytical day. The varying water contents of the standards allows for the production of a calibration line, (Fig. S1), which was used to estimate the water content of the unknowns based on their $^{1}H^{-}/^{18}O^{-}$ ratio (Eqn. 2).

$$H_2O \text{ wt.\%} = (^{1}H^{-}/^{18}O^{-}) \times \text{line slope} \qquad \text{[eqn.2]}$$

As the calibration line was forced through the origin the intercept on the y-axis is zero. An anhydrous San Carlos (SC) olivine standard (kept in a vacuum oven at 60 °C prior to analysis) was used to determine instrumental detection limit during the analytical run, which was 1 ppm. The H_2O detection limit on each NWA 11522 sample was estimated in a similar way, using the $^{1}H^{-}/^{18}O^{-}$ ratios of pyroxene and plagioclase feldspar, both nominally anhydrous minerals. The H_2O detection limit calculated via an analysis of pyroxene within the epoxy-mounted sample NWA 11522(Ep) was 190ppm. To check if this was due to sample degassing from the epoxy resin a nearby feldspar (plagioclase) grain was analysed, which produced a lower water content of 77 ppm (Table 3), suggesting the pyroxene grain may have an indigenous water content. Another pyroxene grain was analysed within the indium mounted sample NWA 11522(In), which was expected to contain a lower background water content due to the anhydrous nature of this sample's preparation. Instead, this pyroxene grain contained an unexpectedly high water content of 465 ppm H_2O. Unfortunately, due to the small nature for this sample, no large pristine feldspar grain could be located for comparison. However, the background H ion counts per second (cps) within the sample chamber were comparable for both epoxy mounted and indium mounted samples (see Table S1 of supplementary materials), again suggesting these pyroxene measurements represent a true water content within the crystal structure, rather than degassing or contamination on the sample surface. Barnes et al. (2020) reported pyroxene water contents of 43 and 61 ppm within paired meteorite NWA 7034, and these background levels were calculated to be between 3 and 29 % of those measured within

the sample apatite grains. Davidson et al. (2020) report water contents of 58-127 ppm on unspecified anhydrous phases within the same meteorite, calculated to be < 20 % of the water content measured within the sample apatite grains. If we assume that pyroxene water content is entirely background, then NWA 11522(Ep) background water content is 4-14 % of the water content within the measured apatite grains. NWA 11522(In) background water content is 9-27 %. Therefore, even with this probable overestimate, background contributions to water content and D/H data are still minor, consistent with previously published data.

The reproducibility of the apatite water contents, and D/H ratios, were calculated based on the subtraction of the true H_2O or D/H value from the estimated H_2O or D/H value of each apatite standard (error = 2*standard deviation (estimated – true)). The 2σ uncertainties of each NWA 11522 apatite H_2O content and D/H ratio were subsequently calculated using the following equation:

$$2\sigma \text{ error} = 2*\sqrt{(\text{individual measurement error}^2 + \text{reproducibility among standard measurements}^2)} \quad \text{[eqn. 3]}$$

To ensure that the SIMS beam was on target, SEM imaging of each analysis area was conducted subsequent to SIMS analyses (see Supplementary Materials). These images revealed that the analysis of apatite 3 within NWA 11522(epoxy) penetrated through to the matrix beneath. As the increase in H counts per second can be tracked through the cycles, for this analysis the last cycles with the beam on (30-35) were discarded as matrix, rather than apatite analysis.

Results

Apatite location and texture

The clastic nature of NWA 11522 is highlighted by SEM-EDS imaging (Fig. 1), with protobreccia clasts, igneous clasts and individual mineral clasts all evident in this polymict breccia. The two samples contain numerous individual mineral clasts of feldspar (<700μm), pyroxene (<600μm, excepting one thermally altered pigeonite grain ~2mm diameter), ilmenite and Fe-oxides (<500 μm) and apatite (<150 μm), with these minerals making up the bulk of the matrix. Our method of calculating modal mineralogy cannot distinguish minerals within the matrix, which was found to make up 65 % and 59 % of NWA 11522(Ep) and

NWA 11522(In), respectively. Pyroxene was found to be the most abundant mineral within the lithic and mineral clasts of both samples, followed by feldspar. Apatite and oxides make up relatively minor components in both samples (Table 1). Agee et al. (2013) reported X-ray diffraction data from NWA 7034, showing that the most abundant mineral is plagioclase (~40%) followed by low Ca-pyroxene (~25%), clinopyroxene (~18%), iron oxides (~9%), alkali feldspars (~5%), and apatite (~3%). The under representation of feldspar within our calculations is almost certainly due to the fact that we were not able to distinguish the matrix minerals, rather than any systematic difference between NWA 7034 and NWA 11522 modal mineralogy. Cl-rich apatite in NWA 11522 is present both within lithological clasts and as free apatite grains within the matrix, as for NWA 7034 (Muttik et al., 2014). However, the largest apatite grains (up to 150 µm diameter) are found within the matrix (Fig. 1).

Table 1: NWA 11522(Ep) and (In) modal mineralogy.

Mineral	NWA 11522(Ep)	2σ	NWA 11522(In)	2σ
oxides	3	<1	2	1
apatite	3	<1	4	1
orthopyroxene	5	1	12	3
clinopyroxene	15	3	7	2
total pyroxene	20	3	19	4
feldspar	9	3	16	4
matrix	65	3	59	2

Apatite volatile abundances

SEM-EDX analyses show that apatite grains within NWA 11522 are Cl-rich (Table 2). Based on 13 anions, stoichiometric calculations were made to determine the ratio of F: Cl: OH in the apatite X-site. Although OH cannot be directly detected via this technique, its abundance can be calculated based on the assumption that only F, Cl and OH are present in the X site (see McCubbin et al., 2013 for details). These abundances are consistent with the previously reported F: Cl: OH range in NWA 7034 apatite (Santos et al., 2013; McCubbin et al., 2016b; Hu et al., 2019; Davidson et al., 2020). Apatite F: Cl: OH ratios are quite closely clustered in NWA 11522 (Fig. 2). No systematic difference is shown between apatite grains hosted within a trachyandesite igneous clast vs. those present as mineral clasts alone within the matrix (Table 2). Again, this is consistent with previously published datasets, where apatite F: Cl: OH was shown to be independent of clastic or matrix associations.

Table 2: NWA 11522 apatite major element composition

	NWA 11522 (In)											
	Apatite 1 + 2 - lithic clast						Apatite 4 - matrix				Apatite 8 - matrix	
	Spectrum 1	Spectrum 2	Spectrum 3	Spectrum 4	Spectrum 7	Spectrum 8	Spectrum 1	Spectrum 2	Spectrum 3	Spectrum 4	Spectrum 1	Spectrum 2
P_2O_5	40.48	40.51	40.02	39.74	38.91	39.32	38.82	40.22	38.87	39.57	39.99	39.89
SiO_2	n.d.	n.d.	n.d.	n.d.	n.d.	n.d.	n.d.	n.d.	n.d.	n.d.	0.24	0.99
TiO_2	n.d.	0.02	n.d.	0.01	0.14	0.03	n.d.	n.d.	n.d.	0.01	0.01	0.03
Al_2O_3	0.12	0.09	0.10	0.16	0.25	0.14	0.30	0.09	0.12	0.12	0.06	0.08
Cr_2O_3	n.d.	0.08	0.01	0.12	0.08	n.d.	0.03	n.d.	n.d.	0.04	0.02	0.06
FeO	0.40	0.65	0.52	0.46	1.28	0.95	0.73	0.57	0.59	0.53	0.73	0.82
MgO	0.05	0.06	0.09	n.d.	0.55	0.16	0.04	0.14	0.27	0.07	0.07	0.45
CaO	54.04	54.11	53.66	53.15	52.39	52.81	52.49	53.50	52.63	53.01	53.37	53.19
Na_2O	0.21	0.24	0.19	0.18	0.16	0.21	0.16	0.23	0.21	0.21	0.23	0.22
K_2O	0.03	0.07	0.06	0.10	0.07	0.04	0.02	0.03	0.03	0.01	n.d.	n.d.
F	0.53	0.35	0.65	0.68	0.69	0.65	0.62	0.25	0.54	0.77	0.86	0.91
Cl	4.75	4.03	4.84	5.18	4.13	5.14	4.47	4.67	5.46	5.30	5.64	5.48
-O ≡ F	0.22	0.15	0.27	0.29	0.29	0.27	0.26	0.11	0.23	0.32	0.36	0.38
-O ≡ Cl	1.07	0.91	1.09	1.17	0.93	1.16	1.01	1.05	1.23	1.19	1.27	1.24
SUM	99.32	99.15	98.77	98.32	97.42	98.00	96.41	98.54	97.28	98.12	99.59	100.50
	Structural Formulae based on 13 Anions											
P	2.99	3.00	2.97	2.96	2.94	2.95	2.96	2.99	2.94	2.96	2.94	2.90
Si	0.00	0.00	0.00	0.00	0.00	0.00	0.00	0.00	0.00	0.00	0.02	0.09
Al	0.01	0.01	0.01	0.02	0.03	0.01	0.03	0.01	0.01	0.01	0.01	0.01
Cr	0.00	0.01	0.00	0.01	0.01	0.00	0.00	0.00	0.00	0.00	0.00	0.00
Ti	0.00	0.00	0.00	0.00	0.01	0.00	0.00	0.00	0.00	0.00	0.00	0.00
Fe	0.03	0.05	0.04	0.03	0.10	0.07	0.05	0.04	0.04	0.04	0.05	0.06
Mg	0.01	0.01	0.01	0.00	0.07	0.02	0.01	0.02	0.04	0.01	0.01	0.06
Ca	5.05	5.07	5.04	5.02	5.00	5.01	5.06	5.04	5.04	5.01	4.97	4.90
Na	0.02	0.02	0.03	0.03	0.03	0.04	0.03	0.04	0.04	0.04	0.04	0.04
K	0.00	0.00	0.01	0.01	0.01	0.00	0.00	0.00	0.00	0.00	0.00	0.00
∑ Cations	8.10	8.16	8.11	8.08	8.18	8.11	8.14	8.14	8.11	8.07	8.04	8.05
F‡	0.15	0.10	0.18	0.19	0.19	0.18	0.18	0.07	0.15	0.22	0.24	0.25
Cl	0.70	0.60	0.72	0.77	0.62	0.77	0.68	0.70	0.83	0.79	0.83	0.80
∑ X-site	0.85	0.69	0.90	0.96	0.82	0.95	0.86	0.77	0.98	1.01	1.07	1.04
OH†	0.15	0.31	0.10	0.04	0.18	0.05	0.14	0.23	0.02	0.00	0.00	0.00

Table 2 (cont.): NWA 11522 apatite major element composition

	NWA 11522 (epoxy)						
	Apatite 5 - matrix	Apatite 7 - matrix				Apatite 8 - matrix	
	Spectrum 2	Spectrum 1	Spectrum 2	Spectrum 3	Spectrum 4	Spectrum 1	Spectrum 2
P_2O_5	39.33	39.28	39.87	39.51	40.22	38.70	38.95
SiO_2	0.44	0.26	0.19	0.23	0.19	0.40	0.32
TiO_2	n.d.	n.d.	n.d.	n.d.	n.d.	n.d.	n.d.
Al_2O_3	0.10	0.05	n.d.	0.06	0.02	0.05	0.02
Cr_2O_3	n.d.	n.d.	0.11	0.04	0.08	0.05	0.08
FeO	0.84	0.62	0.55	0.57	0.56	0.55	0.59
MgO	0.04	0.08	n.d.	0.04	0.06	0.04	0.06
CaO	52.59	52.79	53.39	52.97	53.58	52.55	52.51
Na_2O	0.15	0.28	0.27	0.24	0.16	0.22	0.18
K_2O	0.04	n.d.	n.d.	n.d.	n.d.	0.01	0.02
F	0.69	0.75	0.43	0.40	0.52	0.62	0.60
Cl	5.24	5.11	4.93	5.29	4.82	5.02	5.21
-O ≡ F	0.29	0.31	0.18	0.17	0.22	0.26	0.25
-O ≡ Cl	1.18	1.15	1.11	1.19	1.09	1.13	1.17
SUM	97.99	97.75	98.44	98.00	98.91	96.80	97.12
	Structural Formulae based on 13 Anions						
P	2.94	2.95	2.97	2.96	2.98	2.94	2.94
Si	0.04	0.02	0.02	0.02	0.02	0.04	0.03
Al	0.01	0.01	0.00	0.01	0.00	0.01	0.00
Cr	0.00	0.00	0.01	0.00	0.01	0.00	0.01
Ti	0.00	0.00	0.00	0.00	0.00	0.00	0.00
Fe	0.06	0.05	0.04	0.04	0.04	0.04	0.04
Mg	0.00	0.01	0.00	0.00	0.01	0.00	0.01
Ca	4.98	5.01	5.04	5.02	5.02	5.04	5.02
Na	0.03	0.05	0.05	0.04	0.03	0.04	0.03
K	0.00	0.00	0.00	0.00	0.00	0.00	0.00
∑ Cations	8.07	8.09	8.12	8.10	8.10	8.11	8.09
F‡	0.19	0.21	0.12	0.11	0.14	0.17	0.17
Cl	0.78	0.77	0.73	0.79	0.71	0.76	0.79
∑ X-site	0.98	0.98	0.85	0.91	0.86	0.94	0.96
OH†	0.02	0.02	0.15	0.09	0.14	0.06	0.04

†OH calculated by assuming F + Cl + OH = 1

‡If F + Cl > 1, F was calculated assuming 1 - Cl = F based on the stoichiometric limit of monovalent anions in the apatite X-site.

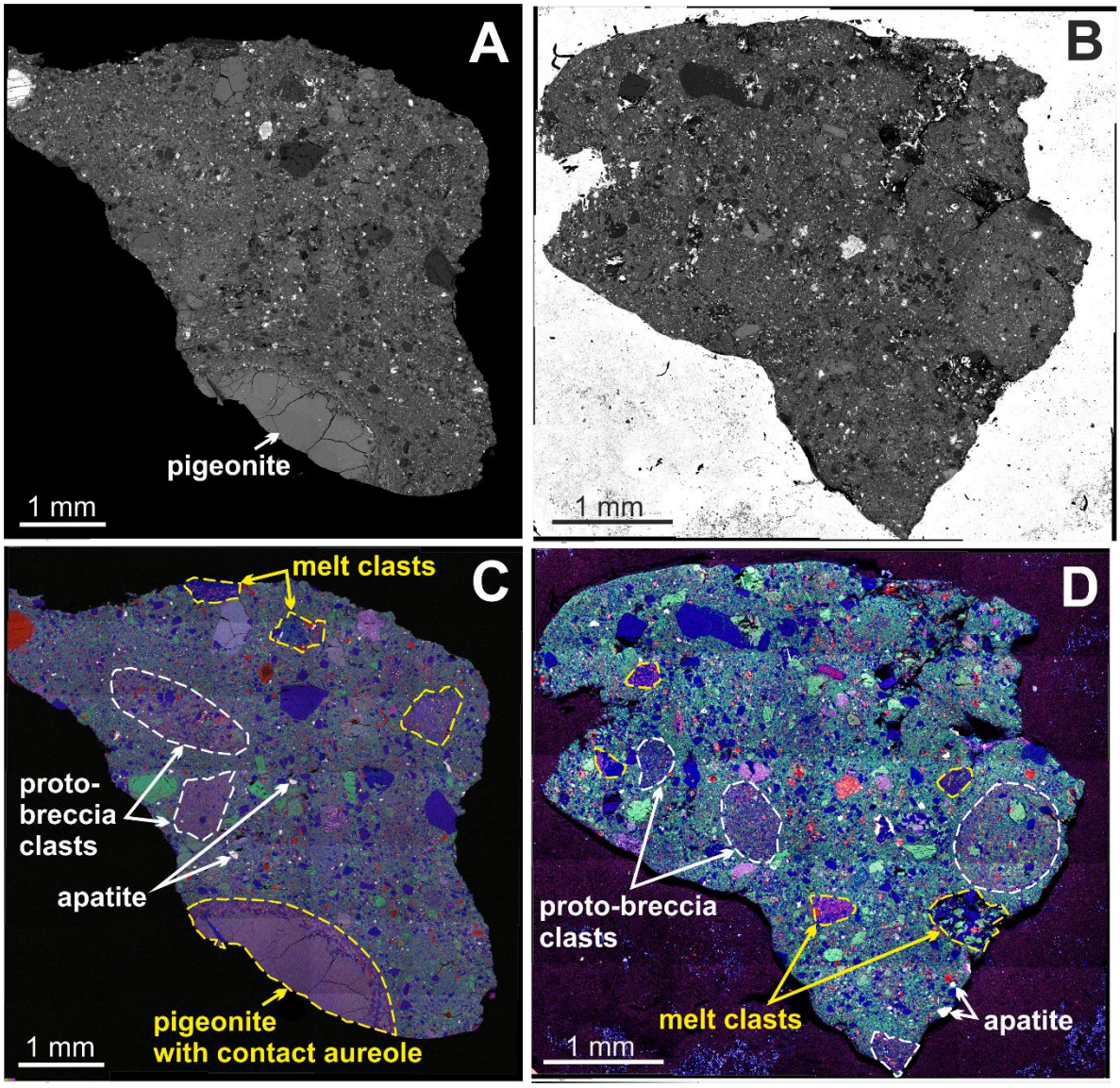

Fig. 1: SEM backscattered electron images (A-B) and EDS false colour images (C-D) of both the epoxy mounted (A,C) and indium mounted (B,D) samples of NWA 11522. For the EDS images: Fe = red, Mg = green, Si = blue, Ca = pink and P = yellow. Orthopyroxene and/or olivine therefore = green, clinopyroxene (including the large pigeonite grain in C) = pink, feldspars = purple or blue, glass = blue, Fe-oxides = red, and apatite = white. The most obvious proto-breccia clasts (white dashed line) and igneous clasts (yellow dashed line), are highlighted.

Hydrogen isotope ratios

Eight apatite grains were analysed for hydrogen isotope ratios, four from NWA 11522(In) (apatite 1,2,4 and 8 in Table 3) and four from NWA 11522(Epoxy) (apatite 3,5,7

and 8 in Table 3). These grains were selected based on size and surface texture (an area >25 µm free of cracks or inclusions is ideal for SIMS D/H analyses). Two of the apatite grains analysed (apatite 1 and 2 in NWA 11522(In)) were contained within a trachyandesite igneous clast, the remainder were present as separate mineral clasts within the breccia matrix.

Apatite hydrogen isotope ratios range between δD 52 ‰ and 782 ‰, with water contents of between 0.127 and 0.510 wt % (Table 3). There is no apparent difference in D/H ratio between apatite grains within the igneous clast (δD = 264-513 ‰) and those present as single mineral clasts (δD = 52-782). Nor is there any D/H ratio distinction between anhedral or subhedral grain textures. At first glance there appear to be two distinct groupings within our dataset (Fig. 3). Group 1 consists of apatite (In)4 and 8 and (epoxy) 3 and 8, characterised by relatively high δD values (782-557 ‰) paired with low water contents (0.184-0.127 wt %). Group 2 consists of apatite (In)1 and (epoxy) 5 and 7, with lower δD values (513-52 ‰) and higher water contents (0.510-0.408 wt %). However, when compared to previously published data (Hu et al., 2019; Barnes et al., 2020; Davidson et al., 2020) our data form part of a mixing line between a high δD (2459 ‰) and low water content (0.030 wt %) endmember, and a low δD (50 ‰) and high water content (0.820 wt %) endmember (Fig. 3).

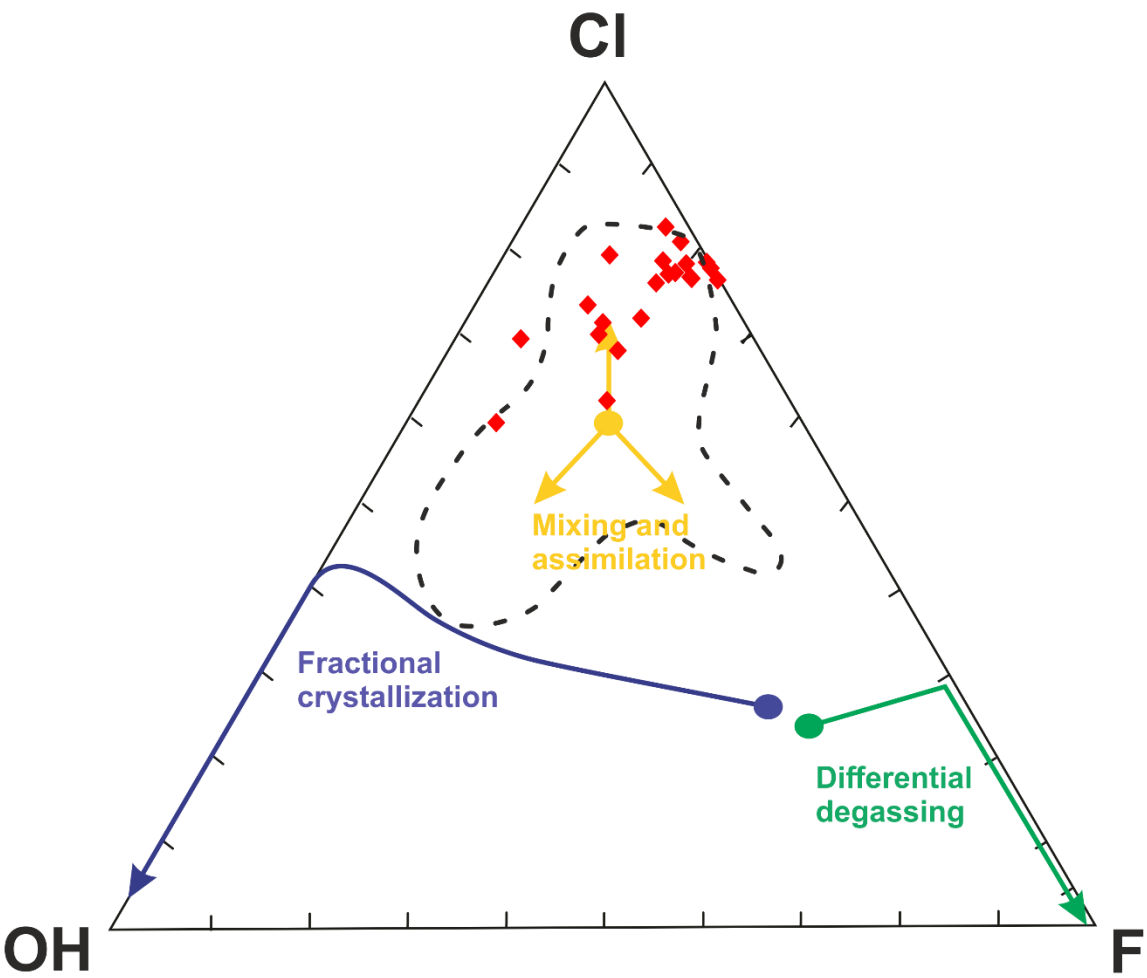

Fig 2: Ternary plot showing measured NWA 11522 apatite Cl: F: OH ratios (red diamonds). Our measured NWA 11522 ratios are comparable to previously reported ratios from NWA 7034 apatite (dashed line envelope - Santos et al., 2013; McCubbin et al., 2016b; Hu et al., 2019; Davidson et al., 2020). Trendlines from McCubbin et al. (2016b) show calculated apatite compositional evolution during mixing/assimilation, fractional crystallization, and degassing.

Table 3: Hydrogen isotope ratios (δD) and water contents (wt %) for apatite grains and anhydrous minerals.

Sample	Texture	δD (‰)	2σ	H_2O (wt.%)	2σ
NWA 11522 (In)					
Apatite 1	LC* - anhedral	513	82	0.436	0.09
Apatite 2	LC - anhedral	264	82	0.510	0.10
Apatite 4	anhedral	782	83	0.182	0.04
Apatite 8	subhedral	631	85	0.171	0.03
NWA 11522 (Epoxy)					
Apatite 3	subhedral	617	84	0.124	0.03
Apatite 5	subhedral	52	82	0.468	0.09
Apatite 7	anhedral	391	82	0.408	0.08
Apatite 8	subhedral	557	84	0.138	0.03
Anhydrous minerals					
Pyroxene (Epoxy)	euhedral	-98	88	0.019	0.004
Pyroxene (Indium)	subhedral	-136	88	0.047	0.001
Plagioclase (Epoxy)	subhedral	133	88	0.008	0.002

*LC = lithic clast, the same igneous trachyandesite clast for both apatite 1 and 2.

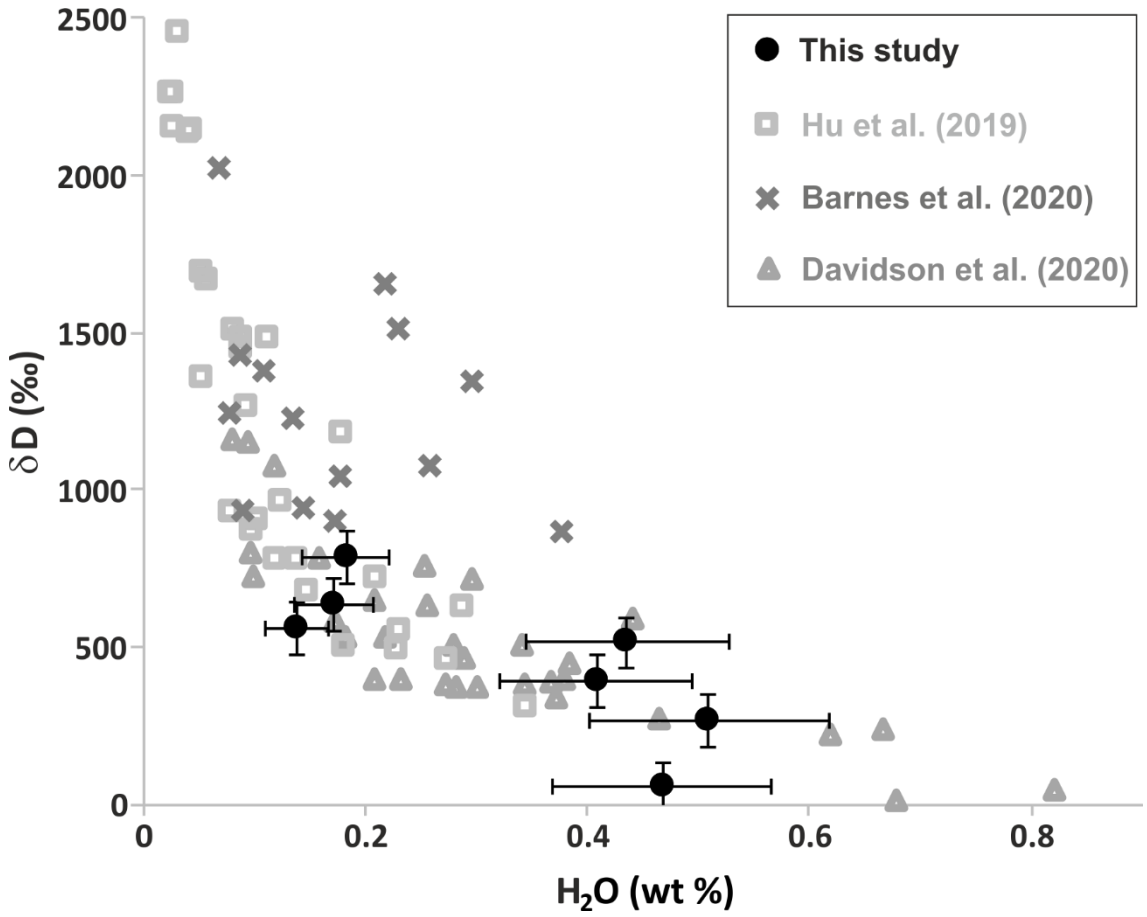

Fig 3: Apatite D/H ratio (δD) versus water content (H_2O wt %). Data from this study (black circles) is in line with that of previous studies, showing a mixing line between a D-rich, water poor endmember and a D-poor, water-rich endmember. Error bars show 2σ uncertainties.

Discussion

Volatile abundances in NWA 11522 and NWA 7034 apatite

Apatite grains within NWA 11522 are consistently Cl-rich, similar to previously published apatite data from NWA 7034 (Santos et al., 2013; McCubbin et al., 2016b; Hu et al., 2019; Davidson et al., 2020). The homogeneity of NWA 11522 and NWA 7034 apatite is uncharacteristic for a polymict breccia, so how might these similar apatite compositions be produced?

Fractional crystallization pathways calculated by McCubbin et al. (2016b) show that, as crystallization progresses, apatite compositions become progressively more OH-rich (Fig. 2). Degassing melts produce progressively more F-rich apatite. Apatite compositions can

only become more Cl-rich during mixing or assimilation. The F: Cl: OH ratios calculated for NWA 11522 apatite, as well as all previously published NWA 7034 apatite data, thus indicate mixing/assimilation due to the dominance of Cl.

One explanation for this could be that this breccia gained its lithic and mineral clasts from several lithologies with similar F, Cl and OH ratios on Mars. Assimilation of a Cl-rich fluid, or mixing of a Cl-rich melt component, could have produced the Cl-dominated apatite within these lithologies (Fig. 2). Alternatively, the volatile content of these apatite grains represents that present during the thermal event that lithified NWA 11522 and its paired stones (McCubbin et al., 2016a,b). As mentioned above, NWA 7034 is reported to contain recrystallized matrix as a result of a thermal event at 1.5 Ga, which produced temperatures of 500-800 °C (McCubbin et al., 2016a). Apatite can crystallise during thermal metamorphism on Earth (e.g., Deer et al., 1992), but the apatite grains within the matrix of NWA 11522 and NWA 7034 are mineral clasts (up to 150 µm diameter) – they do not form part of the 120° triple junction structure seen in the fine grained recrystallized matrix. In addition, apatite mineral clasts within the matrix do not show a distinct difference in volatile content compared to apatite grains within lithic clasts, and there is no systematic difference in texture. This textural evidence suggests that all apatite grains were crystallised prior to 1.5 Ga, but the volatile content and U-Pb ages of the grains could have been reset during the thermal event at 1.5 Ga – especially if fluid was present.

Hydrous Fe-oxides have been identified in NWA 7034 and pairs, in addition to magnetite, maghemite and 1-2 wt % phyllosilicate (saponite) within the matrix (Gattacceca et al., 2014; Muttik et al., 2014; Wittman et al., 2015). Such an alteration assemblage is indicative of low temperature hydrothermal alteration within the breccia after matrix recrystallisation. The fresh condition of NWA 7034 fusion crust, along with the oxygen isotope composition of the water within the alteration phases, argues against significant terrestrial weathering and suggests these alteration phases were produced on Mars (Agee et al., 2013; Muttik et al., 2014). This is in agreement with our textural and mineralogical investigations of NWA 11522, which show no evidence of pervasive terrestrial alteration within either sample of NWA 11522 (e.g., calcite or sulphate veins). Textural evidence also suggests that a number of protobreccia clasts contain martian phyllosilicate produced before breccia formation (McCubbin et al., 2016a). Thus, fluid was present within the breccia before and after the thermal lithifying event on Mars, hence was probably also present during this event.

NWA 11522 and NWA 7034 apatite D/H ratios

Hydrogen isotope data can help determine whether primary lithological similarities or secondary volatile resetting is most likely to have produced the apatite volatile contents in NWA 11522 and its paired stones. Our apatite D/H data, along with previously published apatite D/H data from paired meteorite NWA 7034, produce a mixing line between two endmembers – one with a high δD and low water content, and the other with a low δD and high water content (Fig. 3). Our highest measured δD = 783 ‰ is similar to that of Davidson et al. (2020) at 1164 ‰. However, both Hu et al. (2019) and Barnes et. al. (2020) report a small number of higher δD values, between 2000 and 2500 ‰. The D/H data of Hu et al. (2019) was produced via NanoSIMS analyses, allowing for a smaller spot size on the sample surface, and thus distinction between apatite core and rim during analysis. For the grains where both core and rim were analysed (n=8), five had cores with higher D/H ratios and lower water contents than the rims. In particular, an analysis profile was taken across one large grain with central merrillite surrounded by apatite, the apatite becoming more D-poor and water-rich towards the rim (core δD = 2265 ‰, rim = 938 ‰). Hu et al. (2019) used this data, alongside U-Pb and Cl isotope data, to argue that the volatile contents of apatite cores in NWA 7034 represent a D-, P-, and ^{37}Cl-rich fluid metamorphic event around ~1.6 Ga on the near surface of Mars – firmly linking apatite volatile content to the thermal event that recrystallised the matrix (McCubbin et al., 2016a). Hu et al. (2019) reasoned that lower apatite rim D/H ratios and increased water contents represent a second, later D- and ^{37}Cl-poor infiltrating fluid, probably sourced from the Martian interior. Mixing of these two martian endmember fluids, the earlier D-rich and water-poor and the later D-poor and water-rich, are in line with our apatite dataset. Thus, D/H ratio zoning within single apatite grains argues against breccia formation from several lithologies with similar volatile contents, as a single fluid source would be required to create such similarity.

Because NWA 11522 and NWA 7034 were collected from the Northwest African desert some time after they fell, is it possible that the low δD and high water content endmember of the mixing line is the product of terrestrial weathering? As mentioned previously, no evidence of pervasive terrestrial alteration is visible within either sample of NWA 11522 analysed during this study, and previous investigations of NWA 7034 secondary mineral assemblages indicate a martian origin (Agee et al., 2013; Muttik et al., 2014). Therefore, we assume the terrestrial weathering effect on apatite D/H and water content to be

minimal. Alternatively, contamination during sample preparation could also produce a low δD and high water content endmember. Within our dataset the apatite grain with lowest δD value and a high water content was measured in the NWA 11522(epoxy) sample (apatite 5). The SEM image for the apatite 5 SIMS pit does not indicate any phase overlap or inclusion of cracks within the analysis. It is therefore difficult to dismiss this datapoint as compromised by epoxy contamination. The dataset of Davidson et al. (2020) contains two datapoints with lower δD and higher water contents than any within our dataset (Fig. 3), despite the careful anhydrous sample preparation and indium mounting described by the authors. Therefore, all available D/H datasets point towards a low D/H ratio and high water content endmember with a martian origin. The most probable source of low D/H fluid at or near the surface of Mars would be degassing water (Wang and Hu, 2020), which could have been produced locally via hydrothermal vents after the breccia-lithifying thermal event at 1.5 Ga. Petrologic investigations of NWA 11522 and NWA 7475 suggest this thermal event was impact related (Daly et al., 2018; Wittman et al., 2015). Therefore, the apatite low D/H endmember within this breccia represents direct evidence of an impact-related hydrothermal system on Mars during the Amazonian period.

Conclusions

Our analyses of apatite grains in polymict breccia NWA 11522 indicate they are Cl-rich, with D/H ratios showing a mixing line between δD 52 ‰ and 782 ‰. These results are consistent with previously published data for paired meteorite NWA 7034. The high D/H ratio endmember represents the a Cl-rich fluid that was present during the thermal (probably impact) event that lithified the breccia at 1.5 Ga. This fluid was probably produced from crustal water or ice within the impacted lithologies. The lower D/H ratio endmember represents a second fluid from the interior of Mars, which interacted with the breccia after lithification. This later fluid likely represents an impact-related hydrothermal system on Mars during the Amazonian period.

Acknowledgements

We would like to thank Peter Chung at the University of Glasgow for his help with SEM and EDS quantification. We would also like to thank reviewers Dr. Jemma Davidson and Dr. Justin Filiberto for their helpful comments and suggestions, as well as associate editor Cyrena Goodrich.

References

Agee, C. B., Wilson, N., McCubbin, F., Ziegler, K., Polyak, V., Sharp, Z., Asmerom, Y., Nunn, M., Shaheen, R., Thiemens, M., Steele, A., Fogel, M., Bowden, R., Glamoclija, M., Zhang, Z. and Elardo, S. 2013. Unique Meteorite from Early Amazonian Mars: Water-Rich Basaltic Breccia Northwest Africa 7034. *Science*, 339: 780-785.

Barnes J.J., McCubbin F. M., Santos A. R., Day J. M. D. Boyce J. W., Schwenzer S. P., Ott U., Franchi I. A., Messenger S., Anand M. and Agee C.B. 2020. Multiple early-formed water reservoirs in the interior of Mars. *Nature Geoscience.* https://doi.org/10.1038/s41561-020-0552-y

Cartwright, J., Ott, U., Herrmann, S. and Agee, C. 2014. Modern atmospheric signatures in 4.4 Ga Martian meteorite NWA 7034. *Earth and Planetary Science Letters* 400: 77-87.

Cohen B. E., Mark D. F., Cassata W. S. Lee M. R., Tomkinson T. and Smith C. L. 2018. Taking the pulse of Mars via dating of a plume-fed volcano. *Nature Communications* 8: 640.

Daly L., Lee M .R., Cohen B. E., Cairney J., Eder K., Yang L., Cox M. A. and Cavosie A. J. 2018. High pressure excursions in the matrix of martian meteorite North West Africa (NWA) 11522. *81st Annual Meeting of the Meteoritical Society*, abstract # 6237.

Davidson J., Wadhwa M., Hervig R. L., Stephant A. (2020) Water on Mars: Insights from apatite in regolith breccia Northwest Africa 7034. *Earth and Planetary Science Letters* (in press).

Filiberto J. and Treiman A. H. 2009. Martian magmas contained abundant chlorine, but little water. *Geology* 37:1087–1090.

Filiberto J., Gross, J. and McCubbin, F. 2016. Constraints on the water, chlorine, and fluorine content of the Martian mantle. *Meteoritics & Planetary Science* 51: 2023-2035.

Filiberto J., McCubbin F. M. and Taylor G. J. (2019), Chapter 2 - Volatiles in Martian Magmas and the Interior: Inputs of Volatiles Into the Crust and Atmosphere, in *Volatiles in the Martian Crust*, edited by J. Filiberto and S. P. Schwenzer, pp. 13-33, Elsevier.

Gattacceca, J., Rochette, P., Scorzelli, R. B., Munayco, P., Agee, C., Quesnel, Y., Cournede, C., and Geissman J. 2014. Martian meteorites and Martian magnetic anomalies: A new perspective from NWA 7034. *Geophys. Res. Lett.* 41: 4859–4864.

Goderis, S., Brandon, A., Mayer, B. and Humayun, M. 2016. Ancient impactor components preserved and reworked in martian regolith breccia Northwest Africa 7034. *Geochimica et Cosmochimica Acta*, 191: 203-215.

Greenwood, J., Blake, R. and Coath, C. 2003. Ion microprobe measurements of $^{18}O/^{16}O$ ratios of phosphate minerals in the Martian meteorites ALH84001 and Los Angeles. *Geochimica et Cosmochimica Acta*, 67: 2289-2298.

Gross, J., Filiberto, J. and Bell, A. 2013. Water in the martian interior: Evidence for terrestrial MORB mantle-like volatile contents from hydroxyl-rich apatite in olivine− phyric shergottite NWA 6234. *Earth and Planetary Science Letters*, 369-370: 120-128.

Hallis L. J., Taylor G. J., Nagashima K., Huss G.R. 2012b. Magmatic water in the martian meteorite Nakhla. *Earth and Planetary Science Letters* 359-360: 84-92.

Hallis LJ, Huss GR, Nagashima K, Taylor GJ, Halldórsson SA, Hilton DR, Mottl MJ, Meech KJ, 2015. Evidence for primordial water in Earth's deep mantle. *Science* 350: 795-797.

Howarth, G., Pernet-Fisher, J., Bodnar, R. and Taylor, L. 2015. Evidence for the exsolution of Cl-rich fluids in Martian magmas: Apatite petrogenesis in the enriched lherzolitic Shergottite Northwest Africa 7755. *Geochimica et Cosmochimica Acta*, 166: 234-248.

Hu S., Lin Y., Zhang J., Hao J., Xing W., Zhang T., Yang W. and Changela H. 2019. Ancient geologic events on Mars revealed by zircons and apatites from the Martian regolith breccia NWA 7034. *Meteoritics and Planetary Science* 54(4): 850–879.

Keller J. M., et al. 2006. Equatorial and midlatitude distribution of chlorine measured by Mars Odyssey GRS. *J. Geophys. Res.* 111: E03S08, doi:10.1029/2006JE002679.

Lin, Y. T., Hu, S. and Zhang, T. 2016. U-Pb Dating of Zircon with Petrographic Settings from the Martian Regolith Breccia NWA 7034. *79th Annual Meeting of the Meteoritical Society*, abstract # 6248.

Mathez, E. and Webster, J. 2005. Partitioning behaviour of chlorine and fluorine in the system apatite-silicate melt-fluid. *Geochimica et Cosmochimica Acta*, 69: 1275- 1286.

McCubbin, F. and Jones, R. 2015. Extraterrestrial Apatite: Planetary Geochemistry to Astrobiology. *Elements*, 11: 183-188.

McCubbin, F., Jolliff, B., Nekvasil, H., Carpenter, P., Zeigler, R., Steele, A., Elardo, S. and Lindsley, D. 2011. Fluorine and chlorine abundances in lunar apatite: Implications for heterogeneous distributions of magmatic volatiles in the lunar interior. *Geochimica et Cosmochimica Acta*, 75: 5073-5093.

McCubbin F. M., Hauri E. H., Elardo S. M., Vander Kaaden K. E., Wang J., and Shearer C. K. 2012. Hydrous melting of the Martian mantle produced both depleted, and enriched shergottites. *Geology* 40: 683–686.

McCubbin F. M., Elardo S. M., Shearer Jr. C. K., Smirnov A. Hauri E. H., and Draper D. S. 2013. A petrogenetic model for the comagmatic origin of chassignites and nakhlites: Inferences from chlorine-rich minerals, petrology, and geochemistry. *Meteoritics & Planetary Science* 48: 819–853.

McCubbin, F., Boyce, J., Novák-Szabó, T., Santos, A., Tartèse, R., Muttik, N., Domokos, G., Vazquez, J., Keller, L., Moser, D., Jerolmack, D., Shearer, C., Steele, A., Elardo, S., Rahman, Z., Anand, M., Delhaye, T. and Agee, C. 2016(a). Geologic history of Martian regolith breccia Northwest Africa 7034: Evidence for hydrothermal activity and lithologic diversity in the Martian crust. *Journal of Geophysical Research: Planets*, 121: 2120-2149.

McCubbin F., Boyce J.W., Srinivasan P., Santos A. R., Elardo S. M., Filiberto J., Steele A., and Shearer C. K. 2016(b). Heterogeneous distribution of H_2O in the Martian interior: Implications for the abundance of H_2O in depleted and enriched mantle sources. *Meteoritics and Planetary Science* 51(11): 2036–2060.

Muttik, N., McCubbin, F., Keller, L., Santos, A., McCutcheon, W., Provencio, P., Rahman, Z., Shearer, C., Boyce, J. and Agee, C. 2014. Inventory of H2O in the ancient Martian regolith from Northwest Africa 7034: The important role of Fe oxides. *Geophysical Research Letters*, 41: 8235-8244.

Owen, T., Maillard, J. P., de Bergh, C., Lutz, B. L. 1988. The abundance of HDO and the value of D/H. *Science* 240: 1767–1771.

Patiño Douce, A. and Roden, M. 2006. Apatite as a probe of halogen and water fugacities in the terrestrial planets. *Geochimica et Cosmochimica Acta*, 70: 3173-3196.

Patiño Douce, A., Roden, M., Chaumba, J., Fleisher, C. and Yogodzinski, G. 2011. Compositional variability of terrestrial mantle apatites, thermodynamic modelling of apatite volatile contents, and the halogen and water budgets of planetary mantles. *Chemical Geology* 288: 14-21.

Santos., A. R., Agee, C. B., McCubbin, F. M., Shearer, C. K., Burger, P. V., Sharp, Z. D. and Zimmer, M. 2013. Apatite and Merrillite from Martian Meteorite NWA 7034. *44th Lunar and Planetary Science Conference*, abstract # 2601.

Santos, A., Agee, C., McCubbin, F., Shearer, C., Burger, P., Tartèse, R. and Anand, M. 2015. Petrology of igneous clasts in Northwest Africa 7034: Implications for the petrologic diversity of the martian crust. *Geochimica et Cosmochimica Acta*, 157: 56-85.

Shearer, C. K., Bell, A. S., Burger, P. V., McCubbin, F. M., Agee, C., Simon, J. and Papike, J. J. 2015. The mineralogical record of fO_2 variation and alteration in Northwest Africa 8159 (NWA 8159). Evidence for the interaction between a mantle derived Martian basalt and a crustal component(s). *46th Lunar and Planetary Science Conference*, abstract #1483.

Simon, J. I., Peters, T. J., Tappa, M. J. and Agee, C. B. 2014. Northwest Africa 8159: An ~2.3 Billion Year Old Martian Olivine-Bearing Augite Basalt. *77th Annual Meeting of the Meteoritical Society*, abstract # 5363.

Taylor G. J., Boynton W. V., McLennan S. M. and Martel L. M. V. 2010. K and Cl concentrations on the Martian surface determined by the Mars Odyssey Gamma Ray Spectrometer: Implications for bulk halogen abundances in Mars. *Geophys. Res. Lett.* 37, L12204, doi:10.1029/2010GL043528.

Usui T., Alexander C. M. O'D., Wang J., Simon J. I. and Jones J. H. 2012. Origin of water and mantle–crust interactions on Mars inferred from hydrogen isotopes and volatile element abundances of olivine-hosted melt inclusions of primitive shergottites. *Earth Planet. Sci. Lett.* 357–358: 119–129.

Usui T., Alexander C. M. O'D., Wang J., Simon J. I. and Jones J. H. 2015. Meteoritic evidence for a previously unrecognized hydrogen reservoir on Mars. *Earth Planet. Sci. Lett.* 410: 140–151.

Usui, T. (2019), Chapter 4 - Hydrogen Reservoirs in Mars as Revealed by Martian Meteorites, in *Volatiles in the Martian Crust*, edited by J. Filiberto and S. P. Schwenzer, pp. 71-88, Elsevier.

Villanueva, G. L., Mumma, M. J., Novak, R. E., Kaeufl, H. U., Hartogh, P., Encrenaz, T., Tokunaga, A., Khayat, A. and Smith, M. D. 2015. Strong water isotopic anomalies in the martian atmosphere: Probing current and ancient reservoirs. *Science* 348: 218–221.

Wittmann A., Korotev R. L., Jolliff B. L., Irving A. J., Moser D. E., Barker I. and Rumble D. 2015. Petrography and composition of Martian regolith breccia meteorite Northwest Africa 7475. *Meteoritics and Planetary Science* 50(2): 326–352.

Wright, S., Christensen, P. and Sharp, T. 2011. Laboratory thermal emission spectroscopy of shocked basalt from Lonar Crater, India, and implications for Mars orbital and sample data. *Journal of Geophysical Research*, 116(E9).